FLUCTUATING FORCES AND ROTOR NOISE DUE TO DISTORTED INFLOW

G. Neuwerth, R. Staufenbiel,
A. Kellner, J. Schreier

Technical University of Aachen
Aachen, F. R. G.

Abstract

If the inflow to propellers and rotors is distorted, the fluctuating blade forces will generate an increase of structural loads and noise radiation. Two types of inflow distortions were investigated theoretically and by experiments:
- a ducted rotor whose inflow is distorted by wakes and
- a helicopter tail rotor cutting the tip vortices of the main rotor.

In both cases the distortions will cause fluctuations of the direction and the magnitude of the flow relative to the blades. Applying a Fourier analysis to these velocity fluctuations, the unsteady blade forces and pressures were computed on the basis of two- and three-dimensional theories. The Fourier coefficients of these forces are the basis for the computation of the additional rotor noise emission due to the inflow distortions. Measurements of the unsteady blade pressures and the radiated noise power spectrum are in resonable agreement with the theoretical results.

I. Introduction

To save energy the aircraft propulsion systems of the next generation will increase the mass flow going through the engine. A first step in this direction was the development of turbofan engines. New powerplant concepts with high propulsive efficiency at cruise Mach number 0.8 are based on the use of multi-bladed propellers (prop-fans) driven by a gas turbine. Another important group of flight vehicles that uses rotors for propulsion are the helicopters. Furthermore the great number of aircraft of the general aviation is driven mainly by propellers. Thus, ducted and unducted rotors are becoming more important and interesting. This paper investigates the influence of inflow distortions on the rotor blade forces and on their increased radiated noise theoretically and by experiment. Two types of inflow distortions were considered. One type of inflow distortions are wakes generated by the wing ore by the tail unit (see e. g. the propeller of the Lear Fan 2100 at the rear part of the fuselage). The investigated configuration, shown in Fig. 1, is a ducted rotor integrated in the fuselage.

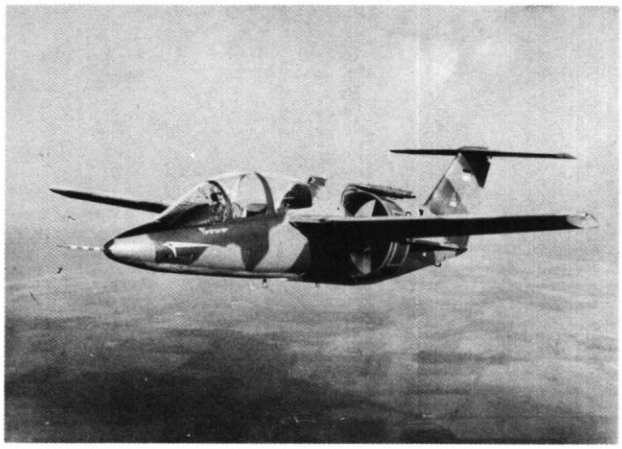

Fig. 1 "Fantrainer" built by Rhein-Flugzeugbau in Germany

The other type of distortions is illustrated in Fig. 2. In this case a tail rotor of a helicopter is influenced by the tip vortices of the main rotor (see Fig. 2).

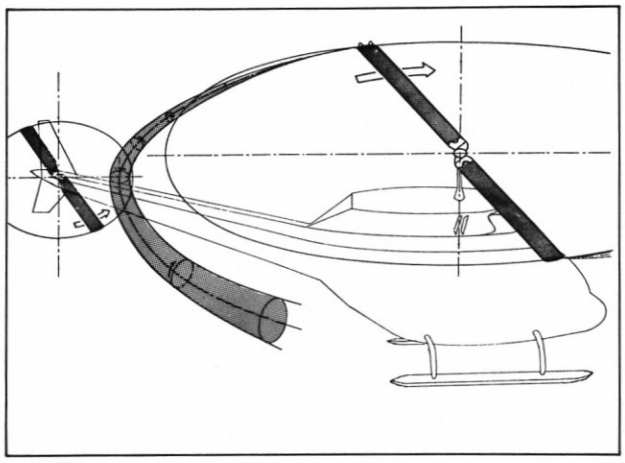

Fig. 2 Interaction of a helicopter main rotor tip vortex with the tail rotor.

During certain flight conditions the tip vortices go through the area of the tail rotor and are cut by the tail rotor blades. In both configurations the inflow distortions lead to velocity fluctuations at the rotating rotor blades. That causes that the effective angle of attack and the dynamic pressure are changed periodically jielding impulsive changes of air-forces and pressures.

After modeling the distortions,the velocity fluctuations could be determined and the unsteady forces and pressures were computed by various theories (see chapter 2). The local blade pressures have also been measured and were compared with the computed values. Outgoing from these forces, as a source of discrete frequency noise, the radiated noise was computed (see chapter 3). In chapter 4 the measured and the theoretically evaluated noise power is discussed including a comparison. For the experiments special rotor test facilities were developed.

2. Computation of the Fluctuating Blade-Forces and Pressures

In Fig. 3 the velocity fluctuations at the location of the blades are shown for the case that the inflow is distorted by a wake.

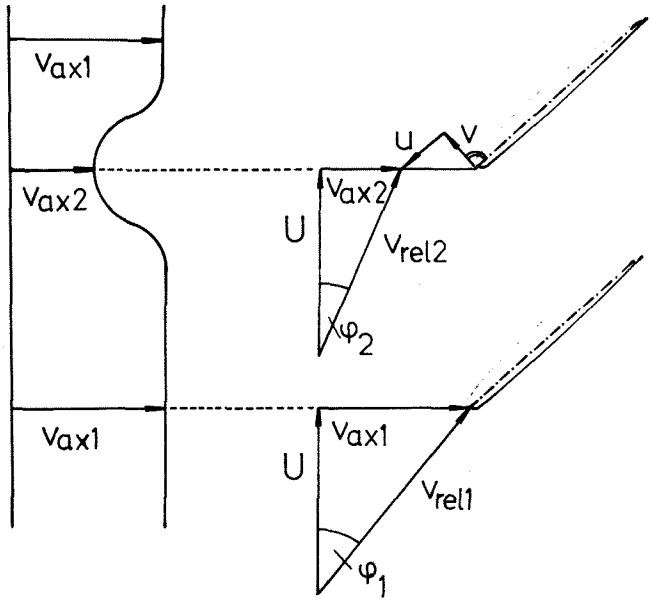

Fig. 3 Inflow distorted by a wake

The change of the axial velocity v_{ax} of the rotor inflow generates mainly a variation of the direction of the relative velocity v_{rel} and a slight change in its magnitude. U is the blade velocity. The wake defect velocity has the two components u longitudinal and v transvers to the blade chord representing the flow perturbations.

Fig. 4 illustrates the other investigated case where the inflow of a tail-rotor is distorted by tip vortices. The flow distortions according to the velocity field of the tip vortex are shown at three different radial positions at the rotor blade. A comparison of the undisturbed relative velocity v_{relun} with v_{rel} shows that both the direction and the magnitude of v_{rel} fluctuate. Fig. 4 presents the simple case that the vortex axis is parallel to the rotor axis. That causes that no flow perturbation normal to the rotor plane exists. In the general case, if the vortex axis is oblique to the rotor axis, flow perturbations normal to the rotor area arise (see chapter 4.2).

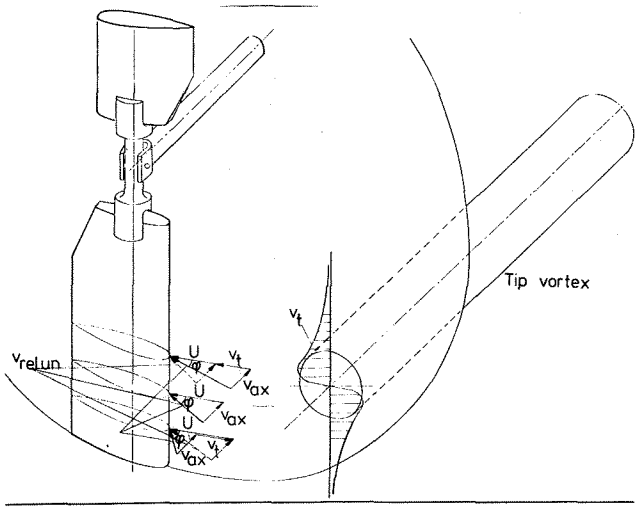

Fig. 4 Fluctuations of air flow speed and -direction on a tail-rotor blade passing a tip vortex (axis normal to the rotor area)

At both types of flow distortions blade forces with strong impulsive fluctuations will be generated. These forces cause mechanical vibrations and an additional acoustic radiation.

In this paper, the theories applied for computing the unsteady blade forces neglect compressibility and friction effects and are based on singularity methods. An early contribution to the unsteady airfoil theory was made by Kemp and Sears (1) reducing the rotor to a two dimensional plane blade row. The interference effects of neighbouring blades are ignored. They computed the unsteady lift of a flat plate only with flow distortions normal to the plate. Horlock (2) determined the lift fluctuations including distortions parallel to the undisturbed flow. Starting from

these theories, Naumann and Yeh (3) developed the unsteady lift for an cambered airfoil that has angle of attack, relative to the steady flow, and velocity distortions normal and parallel to the chord. The airfoil is represented by a vortex sheet situated along the chord (see Fig. 5).

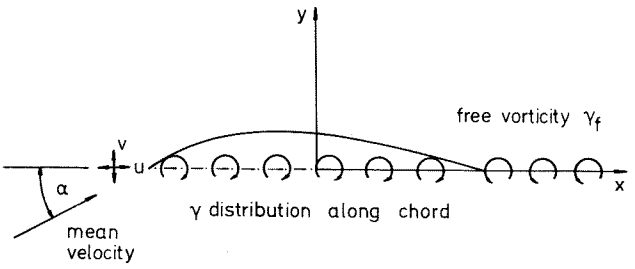

Fig. 5 Distribution of vorticity

The inflow distortions are periodical for the rotating blade. The inflow can be represented by a mean velocity and the Fourier components of the flow disturbances. Due to this inflow, the vorticity γ along the chord consists of a steady and a time dependent vorticity $\gamma = \gamma_{St} + \gamma_{un}$. Due to the variation of the bound vorcity (γ_{un}) free vortices (γ_f) will be shed. It is assumed that they are carried away with the mean velocity along a plane in the direction of the chord. The unsteady vorticities γ_{un} and γ_f induce unsteady velocities at the airfoil. The total flow - the mean flow plus disturbances plus the total induced velocity - must be tangent to the camber for all x values. Using the known relation between γ_{un} and γ_f a connection can be developed between the flow disturbances u and v and the unsteady induced velocities. The result is an integral equation between γ_{un} and the known Fourier components of the flow disturbances u and v. Applying the Euler equation, the unsteady forces can be determined using the computed values of the vorticities.

Additional to the method of Naumann and Yeh a theory of Henderson (4) is applied to compute the unsteady blade forces. This theory includes additionally the interference effects of neighboring blades.
Further, a three-dimensional theory was used for calculating the blade forces of a ducted rotor. This theory was based on the paper of Fathy (5). The blades are allowed to be arbitrarily tapered and twisted, the casing effects considered by a theory of images. The reference blade is replaced by a continuous distribution of vorticity while the other blades are replaced by concentrated radial lines of vortices. The free vortices form a continuous sheet of vorticity. This sheet consists of vortices whose axes are parallel to the trailing edge of the blade - caused by the inflow distortions - and of vortices whose axes are perpendicular to the trailing edge. The latter vortices are generated by the radial variation of circulation. The theory of Fathy was modified by Kellner (6) for including variable velocities at different radial positions. Furthermore, the influence of cambered leading and trailing edges can be calculated.

Besides the blade forces, the unsteady blade pressures were computed for arbitrary points along the chord. These blade pressures are compared with measured values. The theory of Naumann and Yeh was extended in that way that not only the blade forces but also the pressure amplitudes and their phase differences could be computed (see Kellner (6)).

3. Theory of the Emitted Sound Field

The principles of the theory of the aerodynamic noise generation are based on the work of Lighthill (7). He went out from the continuity equation and the equation for the conservation of momentum and developed the basic general wave equation of the aeroacoustic. In this equation three different acoustic source terms are represented. Concerning the rotor noise generation at lower subsonic rotor tip speeds - as regarded in this paper -, two of these source terms are inefficient: that is the effect of mass displacement of the rotating blades and the effect of turbulent momentum exchange in the boundary layers and the wakes of the blades. As the dominant source term the effect of the fluctuating forces F_i^* remains. Now the wave equation can be written as

$$\frac{1}{a_0^2}\frac{\partial^2 p}{\partial t^2} - \frac{\partial^2 p}{\partial x_i^2} = -\frac{\partial F_i^*}{\partial x_i}$$

with the sound pressure p, the speed of sound a_0, the time t und x_i a three-dimensional cartesian coordinate (see Fig. 6).

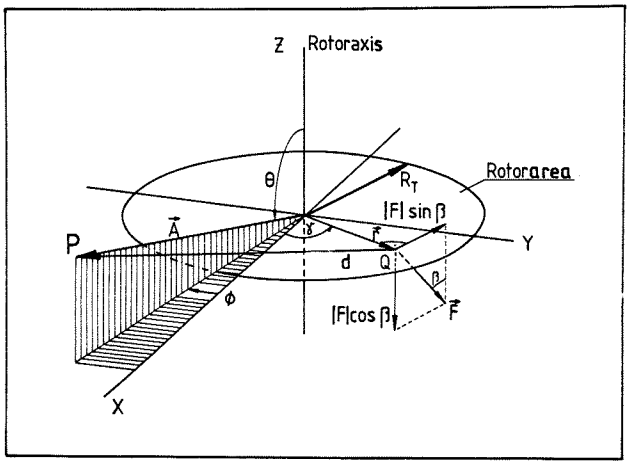

Fig. 6 Coordinates, angle notations and orientation of the force F per unit of rotor area acting on the fixed point in space Q

Lighthill gave the solution of this wave equation in the form

$$p_s = \frac{1}{4\pi} \frac{\partial}{\partial x_i} \int \left[\frac{F_i}{d}\right] dA$$

where p_s is the sound pressure at the position of the observer P. d is the distance from source Q to observer P and dA is an element of the rotor area. F_i are now the components of the force per unit area acting on fixed points in the rotor area. F is generated as the reaction of lift and drag of the rotor blades. The square brackets around F_i/d imply the evaluation at the retarded time $\tau = t - d/a_o$. To integrate over the rotor area requires an integration over the radius R_T and over the angle γ around the rotor.

At first, the fluctuations shall be analysed for a rotor with undisturbed inflow. In this case the blade forces do not change during the revolution. However, there are fluctuations in F_i at a fixed point in space, every time a blade passes by. These fluctuations are periodical with the blade passing frequency b . n, where b is the blade number and n is the rotor rotational speed (see Fig. 7).

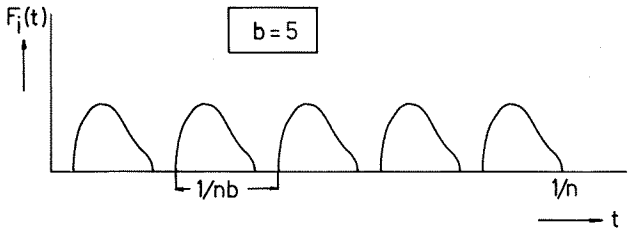

Fig. 7 Fluctuations of F_i at a fixed point in space near the rotor area

These fluctuations can be Fourier analysed having discrete frequencies

$$f_m = m\ b\ n$$

with the harmonic order m. The Fourier coefficients depend on the shape of the F_i-pulses. This shape is determined by the pressure distribution acting on the blade element.

However if the inflow is disturbed, the aerodynamic force K on a blade element which traverses this disturbance is not constant. The fluctuation of K is also periodic the frequency being k · n (see Fig. 8), where k is the number of disturbances which are passed by the blade element during one revolution. Because of the periodicity, k can be Fourier analysed with the Fourier coefficients k_l and the discrete frequencies $f_l = l\ k\ n$ (harmonic order l). Fig. 8 shows the first three harmonics.

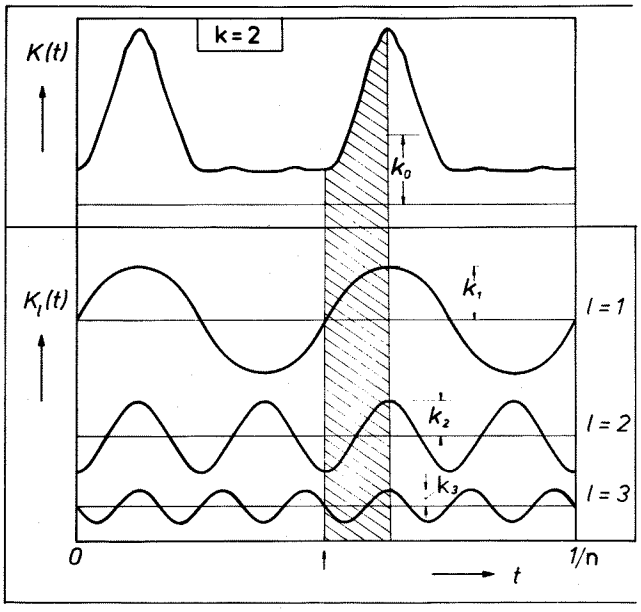

Fig. 8 Force fluctuations acting on a blade element passing two wakes during one revolution

Equivalent to the case of a homogeneous inflow a fixed point in the rotor area sees the reactions $F_i(t)$ which result from the force K(t) acting on that blade element when passing by. The hatched area in Fig. 8 shows the variation of the resulting blade force K and the harmonics with respect to time while passing a fixed point in the rotor area (the width of the hatched area depends on the chord length). The fluctuations of F_i at that fixed point are plotted in Fig. 9 for a five-bladed rotor. Here, the simplifying assumption was made that the pressure distribution should be constant over the chord; in this case the signature $F_i(t)$ could be obtained directly. It can be recognized that every harmonic K_l of the blade force generates a fluctuation F_{il}. All these fluctuations F_{il} are periodic and can be Fourier analysed, the discrete frequencies being $f_m = m\ b\ n$. That has the consequence that every blade force harmonic generates multiple F_i- and sound pressure harmonics.

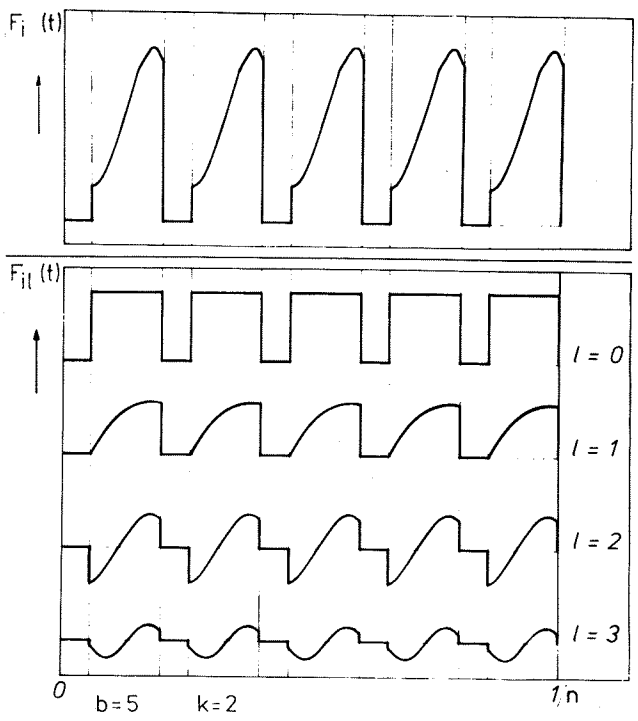

Fig. 9 Fluctuations of F_i at a fixed point in the rotor area according to Fig. 8

To compute the radiated noise of the whole rotor the contributions of the F_i-fluctuations at all fixed points in the rotor area have to be integrated considering the phase relations. Regarding all points situated over a circle at a constant radius it can be seen that the Fourier coefficients of F_{il} are modulated over the circle. This modulation is according to the shape of K_l (see Fig. 8). However all the Fourier components and their phase relations are changing with the radius. This has a great influence especially in case that the inflow is distorted by several tip vortices. To consider this, the existing rotor noise theories of Lowson (8), Ollerhead and Munch (9) and Wright (10) had to be extended. The following equation for the sound pressure harmonics p_m is deduced by Schreier (11):

$$Pm(t,\Phi,\theta)=\frac{mb^2\Omega}{4\pi a_o A}\int_0^{R_T}|X_m(r)|$$

$$\sum_{l=0}^{\infty} J_q(mb\Omega r\sin\phi/a_o)K_l(r)\cdot$$

$$\cdot\{\sin[mb\Omega(t-\frac{A}{a_o})-q_-(\phi-\pi/2)-\varphi_l(r)]$$

$$(\cos\phi\cos\beta-\frac{q_- a_o}{mb\Omega r}\sin\beta)$$

$$+\sin[mb\Omega(t-\frac{A}{a_o})-q_+(\phi-\pi/2)+\varphi_l(r)]$$

$$(\cos\phi\cos\beta-\frac{q_+ a_o}{mb\Omega r}\sin\beta\}dr$$

The angle notations are to be taken from Fig. 6. The amplitudes of the blade force harmonics K_l in the rotating system and their phase differencies φ_l (see Fig. 8) can be evaluated by the theories mentioned in chapter 2. q is the modal order of the sound field with $q_+ = mb + kl$ and $q_- = mb - kl$, Ω the angular velocity of the rotor and J_q is the Bessel function of qth order. X is a spectral function determined by the pressure distribution along the blade chord. Here, the assumption is made that the pressure distribution is independent of the varying value of the resulting blade force. Analysing the equation for the sound pressure harmonics, it can be recognized that every blade force harmonic of order l generates multiple sound harmonics of order m. The directivity pattern of the sound radiation (depending on Φ and θ) can be computed in a numerical way. To make comparisons with measurements the sound power W_m had to be computed by integration of the square of the RMS-values of p_m over a sphere around the rotor:

$$W_m=\frac{1}{T}\int_{t=0}^{T}\int_{\varphi=0}^{2\pi}\int_{\phi=0}^{2\pi}\frac{p_m^2(t,\phi,\theta)}{\varrho_o\, a_o}\,d\theta\,d\phi\,dt$$

where ϱ_o is the density of the surrounding air.

To compute the p_m-values, not only the unsteady blade forces but also the steady values have to be determined. The steady forces were computed with a computer program of the company VFW-Fokker (12) based on the 3-dimensional Goldstein theory.

4. Theoretical and Experimental Results

4.1 Inflow Distorted by Wakes

The experimental investigations were carried out with a rotor-test-facility in the free test section of a subsonic wind tunnel (see Fig. 10). A flight speed v_{oo} can be simulated by the wind tunnel.

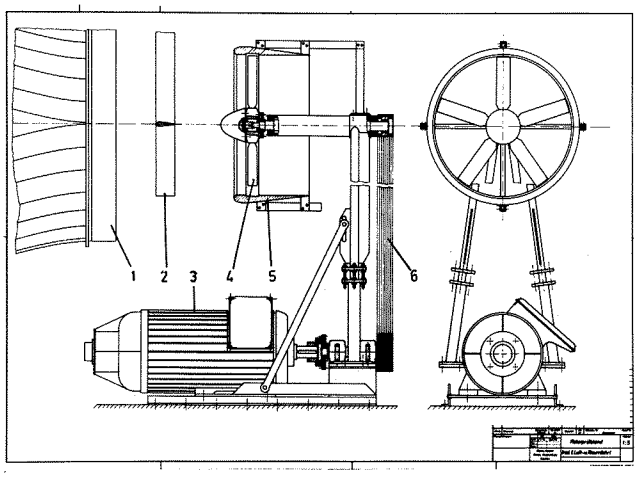

Fig. 10 Rotor-test-facility

1 wind tunnel nozzle (diameter = 1.5 m)
2 profiles to generate different wakes
3 power unit
4 5-bladed rotor (R_T = 0.45 m)
5 rotor duct
6 V-belt drive

In Fig. 11 two of the used profiles with their corresponding wakes measured at the location of the rotor plane are shown. The wakes were measured with running rotor (n = 5000 rpm) and a simulated flight speed v_{oo} = 60 m/s.

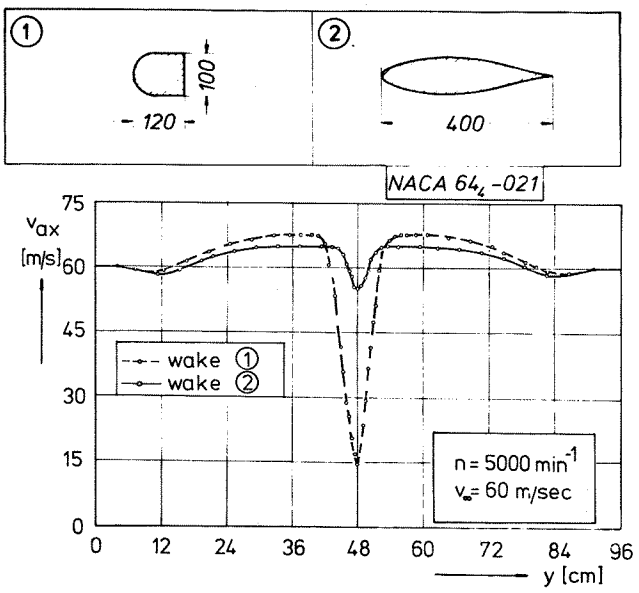

Fig. 11 Wakes of two different profiles in front of the rotor

In front of the rotor the axial velocity v_{ax} is higher than v_{oo} due to the running rotor. The bluff body profile (1) generates a wake of maximum strength with regard to amplitude, loss of momentum and maximum gradient. Starting with the Fourier analysis of these wakes, the unsteady blade forces were evaluated with the theory of Naumann and Yeh. In Fig. 12 the force variation on a blade element is shown for profile (2) - K is the blade force per unit radial length. The force variations during one revolution of the rotor for the radius r/R_T = 0.75 are demonstrated. For comparison, forces calculated with a quasistationary approach are shown in this Figure as well. The unsteady effects reduce the influence of the wake in such a way that the gradient $\partial K/\partial t$ and the amplitude of the force variations are decreased. These unsteady effects depend on the reduced frequency $\omega = \pi c/\lambda_1$ as an important parameter with c as the chord length of the blade and λ_1 as the wave length of the velocity distortions of order 1.

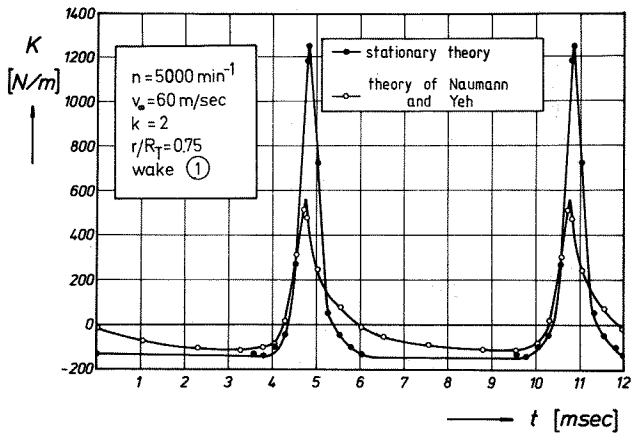

Fig. 12 Force fluctuations on a blade element during one revolution

Fig. 13 compares the unsteady blade forces for the two wakes of Fig. 11 computed with the theory of Naumann and Yeh. It can be seen that the bigger wake (1) generates the stronger force variations.

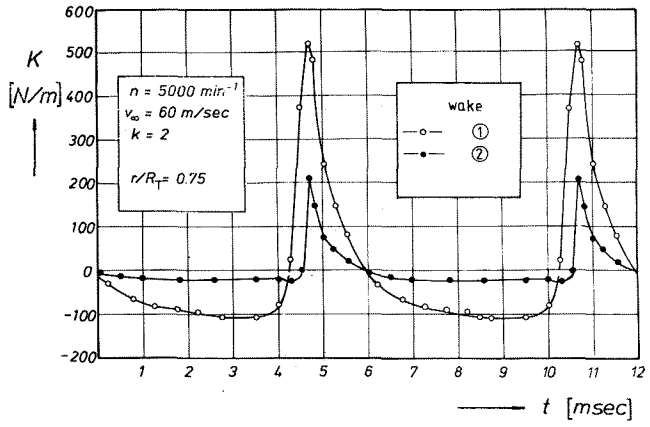

Fig. 13 Force fluctuations on a blade element for two different wakes

The Fourier coefficients $\hat{v}_{axl}$ of the axial velocity distribution of the wake (1) are plotted on the top of Fig. 14 for three different radial positions r/R_T. Additionally the corresponding force harmonics K_l are shown in Fig. 14.

With increasing radius r the same wake - the wake dont changes in the radial direction - covers a smaller position of an increasing circumference $2\pi r$. Therefore, the velocity disturbance gets a more impulsive character leading to an increase of the higher harmonics of v_{ax} with increasing r while the lower harmonics are decreasing. Nevertheless, the lower blade force harmonics are increased with increasing r. This is caused by the unsteady aerodynamic effects. For the same harmonic order l the wavelength of the velocity harmonics becomes larger when the radius and herewith the length of the circumference are increased. That means that the reduced frequency ω is decreased with increasing r. Consequently, the reduction of the blade force amplitudes due to the unsteady aerodynamic effects is diminished for higher values of r. Therefore, at the blade tip the strongest force fluctuations appear.

The unsteady blade forces computed with the theory of Henderson (4) gave, at radial positions $r/R_T > 0.7$, nearly the same results as the theory of Naumann and Yeh. The reason is the relatively high spacing of the 5-bladed rotor.

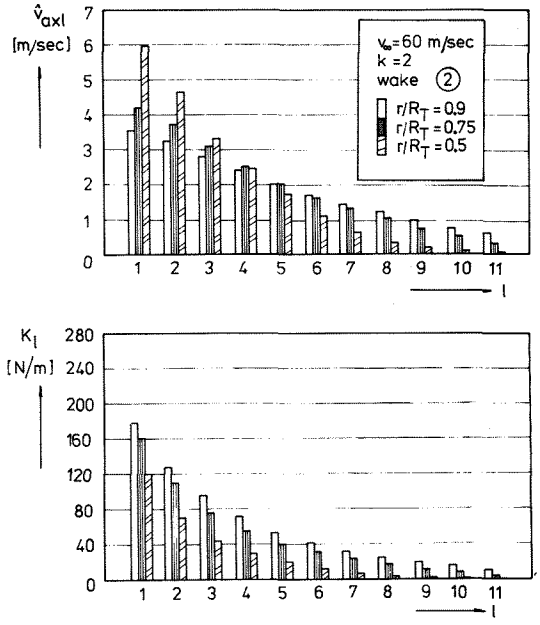

Fig. 14 Fouriercoefficients of the axial velocity of wake and of the corresponding blade forces for three radial positions

As seen in Fig. 14 the Fourier coefficients of the flow fluctuations and of the blade forces depend on the radial position. Therefore, a theory which considers three-dimensional effects will give different results.

Using the 3-D-Theory described in Chapter 2, the blade force fluctuations due to the wake (2) were calculated for five radial positions (see Fig. 15).

It is evident that the force amplitudes grow up with increasing r. The force fluctuations of Fig. 13 can be compared with these results; the radial position $r/R_T = 0.75$ of Fig. 13 corresponds to a value

$$\frac{r - R_i}{R_T - R_i} = 0.67.$$

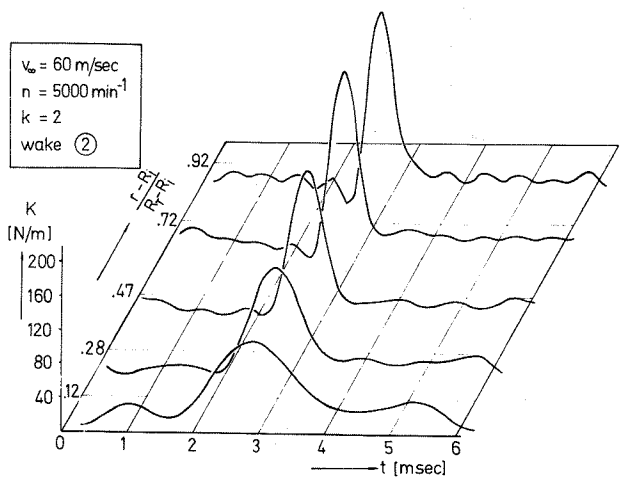

Fig. 15 Blade force fluctuations for 5 radial positions computed with a 3-D theory

(Hubradius: $\frac{R_i}{R_T} = 0.24$)

The local pressure fluctuations on the blades were measured with Kulite pressure transducers. Fig. 16 demonstrates a reduction of the pressures with increasing harmonic order l. In this case the pressures were measured at the radial position r/R_T = 0,5 on the suction side at 9 % of the chord length.

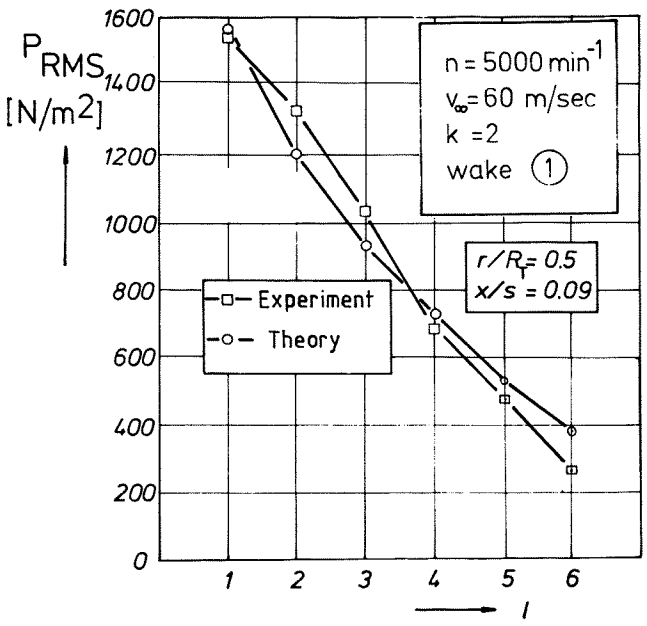

Fig. 16 Comparison of the Fourier coefficients of the computed and measured local blade pressures

Pressure values computed for the same position on the blade (for theory see chapter 2) are in good agreement with the measured data.

The acoustic measurements were limited to the determination of the acoustic power and its spectrum because the laboratory has the characteristic of an reverberation room. To prevent problems with standing waves, caused by discrete frequency noise, the measuring microphone was rotated on a boom and the RMS-values of the radiated sound pressure were averaged for one revolution of the boom. The sound pressures were filtered and averaged and finally, the sound power levels PWL were computed. This evaluation is influenced by the acoustic characteristics of the reverberation room - especially by the absorption area. Fig. 17 gives a comparison of the 1/3-octave analyses of the measured sound power levels for three cases: inflow distorted by wake(1), by wake(2) and the undisturbed case (see Kellner (6)).

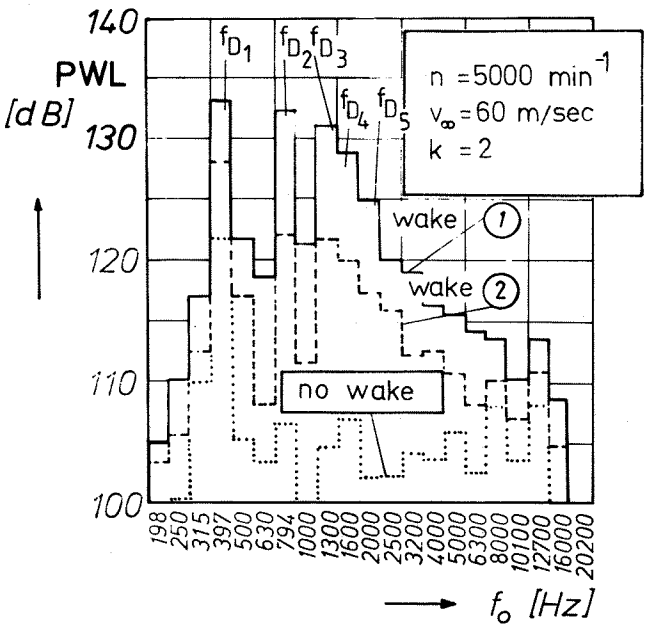

Fig. 17 1/3-octave analysis of the radiated sound power level with and without distorted inflow

The strong influence of the wakes on the increase of the radiated noise is evident. The large wake (1) generates the most additional noise. It can be seen that the interaction with the wakes amplifies especially the PWL-values of the harmonics of the blade passage frequency (f_{D1} = 416.7 Hz). These harmonics are influenced by the fluctuating blade forces. The increase of the higher harmonics causes a strong amplification of the subjective loudness. The special sensitivity of the human ear is considered, if the PWL-values are A-weighted. Fig. 18 demonstrates the increase of the A-weighted over-all sound power level Δ OAPWL for the investigated profiles as a function of the forward speed v_{oo}.

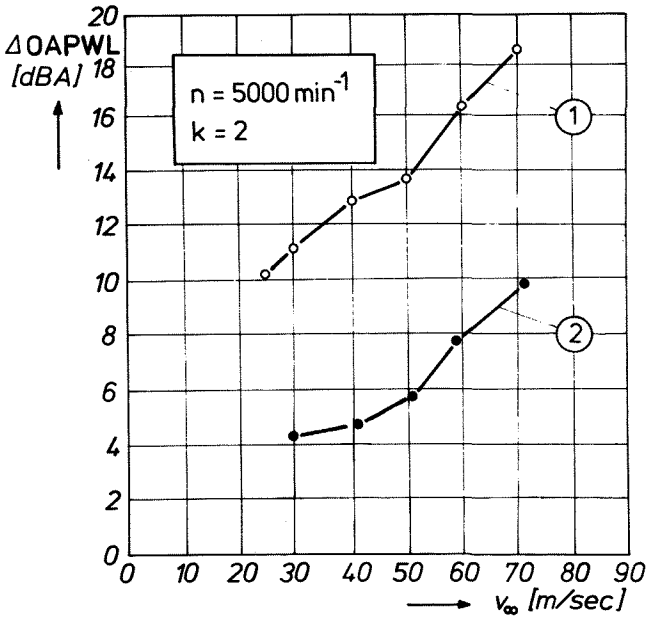

Fig. 18 Additional Δ OAPWL as a function of the forward speed for the two different profiles (see Fig. 11)

The additional over-all sound power level - the difference between the noise with and without wakes - has a value of 16 dBA for the wake (1) at v_{oo} = 60 m/s. This value demonstrates the considerable influence of the harmonics because the sound power level of the blade passage frequency shows only an increase of ablout 10 dBA (see Fig. 17). In Fig. 19 the measured PWL-values are compared with the theoretical values. The unsteady blade forces were computed with the 2-D-Theory of Naumann and Yeh while the forces were evaluated with a stationary program based on the 3-D-Goldstein- theory(VFW-Fokker (12)).

In the case that the inflow is distorted by wakes, the following simplified method of noise computation was applied: in this noise theory no integration over r was done but the computation considered only the resulting force assumed to be located at the "effective" radius r/R_T = 0.75. In Fig. 19 additionally the number k of the wakes was varied. If k is doubled, the over all sound power level is increased by 1.5 to 2 dB. The measured and theoretical values show a fairly good agreement. Most of the measured data show a higher level than the computed ones, because the noise theory does not include the turbulence of the inflow.

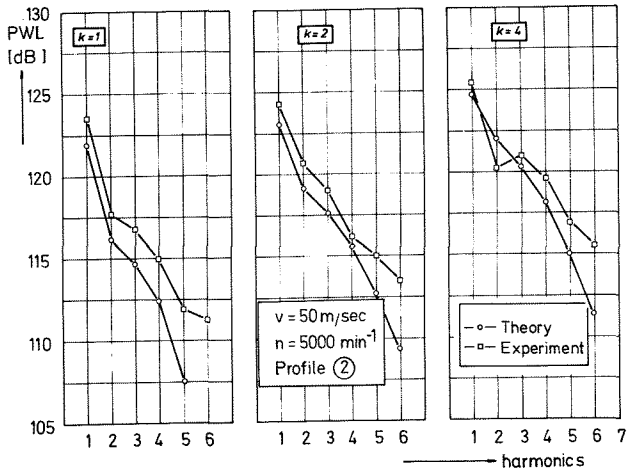

Fig. 19 Computed and measured sound power levels for three different numbers k of wakes

Also the sound source term considering the turbulent momentum exchange in the boundary layers and the wakes of the blades is neglected. These source terms influence, in particular, the higher harmonics (m > 4).

Further, the influence of the shape and the strength of the wake on the radiated noise power was investigated theoretically. The velocity profiles in the wake can be approximated by a bell shaped Gaussian curve. Fig. 20 compares the velocity distribution of the wake 2 with the Gaussian curve whose velocity distribution can be written as

$$v(y) = v_\infty - A e^{(y-y_m)^2/2\sigma^2}$$

The maximum loss of velocity in the wake is at the point y_m. The wake can be described by two parameters: amplitude A and σ, as a measure for the width of the wake. Usually the wake is characterized - besides the amplitude A - by the loss of momentum J_o and the maximum velocity gradient G. These parameters are independent of each other and can be easily calculated, once A und σ are known.

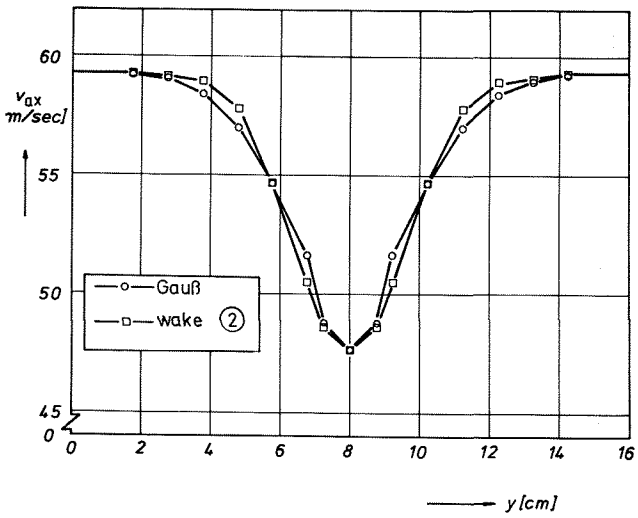

Fig. 20 Approximation of wake (2) by a Gaussian curve

An important result of these noise calculations is shown in Fig. 21. Here the effect of A and J_o on the over-all acoustic power level is demonstrated.

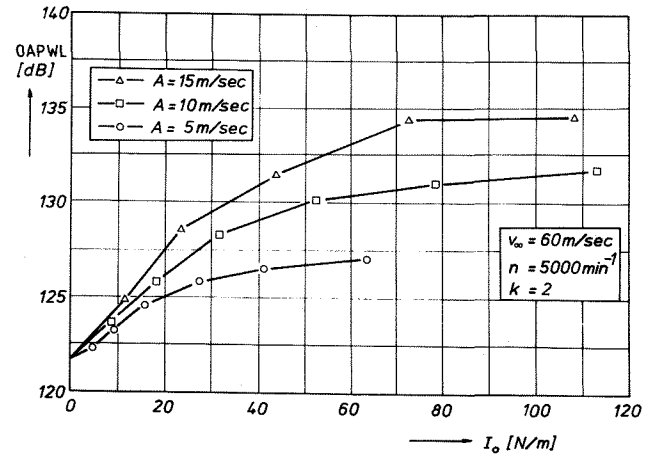

Fig. 21 Over-all sound power level as a function of the loss of momentum in the wakes for three different amplitudes

If J_o is small, the loss of momentum is the main factor in determining the noise radiation. However if J_o is increased, the influence of A dominates. Fig. 22 shows the influence of G on the noise radiation.

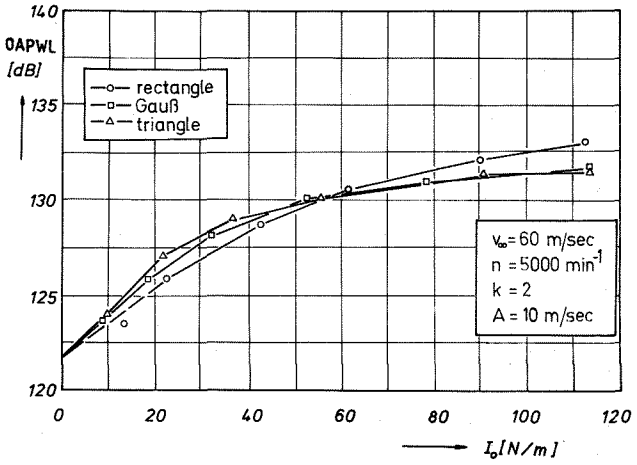

Fig. 22 Over-all sound power level as a function of the loss of momentum in the wakes for three different velocity gradients.

Besides a Gaussian velocity distribution in the wake, triangular and rectangular distributions were also studied. If the distributions have the same amplitude, the influence of the velocity gradient, which differed strongly from case to case, is small.

4.2 Rotor whose Inflow is Distorted by Tip-vortices

To simulate the interaction of the tip vortex of a helicopter main rotor with a tail rotor, a test facility was built consisting of two rotor test plants (see Fig. 23). The tail rotor is the original part of the helicopter Bell UH-1D (blades are not twisted and have a NACA-profile 0012). The second rotor serves as a generator for the tip vortices (one vortex spiral and the intersection areas with the tail rotor are illustrated). This test arrangement sumulates in principle the interaction at a helicopter (compare Fig. 2).

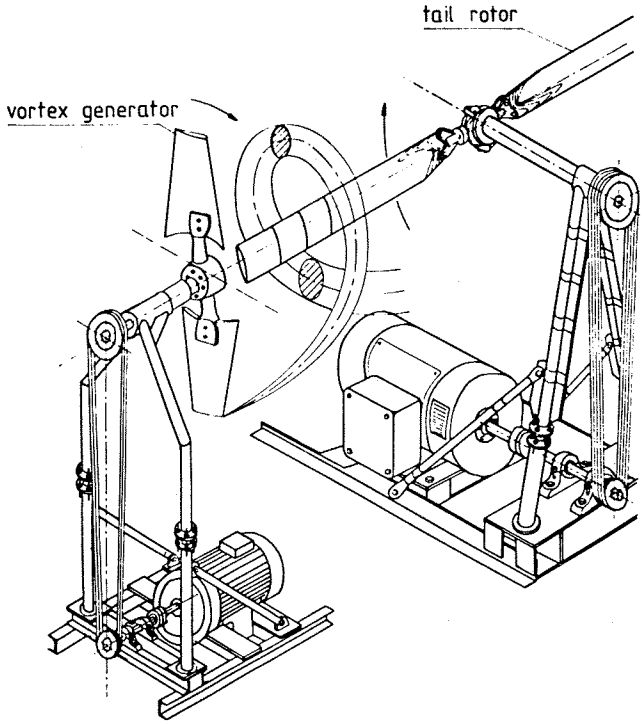

Fig. 23 Arrangement of the tail rotor test plant

A vortex intersecting the tail rotor area induces at every point Q in the rotor area a velocity v_t whose direction and magnitude depends on the distance between Q and the axis of the vortex. Further on, the orientation of the direction of this axis influences the components u and v of the induced velocity. v is the component in the rotor area normal to the leading edge of the blade, while u is the component normal to the rotor area. The components of the flow perturbations parallel to the leading edge are not regarded because they have a very low influence on the blade forces. While in Fig. 2 the simple case was demonstrated that the vortex axis is normal to the rotor area - there exists only the component v -, Fig. 24 represents the general case. The orientation of the axis is given by the angles ξ_c and η_c, where ξ_c is the angle between the rotor area and the vortex axis and η_c is the angle between the projection of this axis into the rotor area and the x-axis. The position of the vortex is determined by the radius r_Γ and the angle χ. The components u and v of the velocity perturbations are computed for every blade element of the rotor - the point Q is situated in the leading edge of the blade elements. This computation is done in a coordinate system that is fixed on the blade element and whose origin is Q.

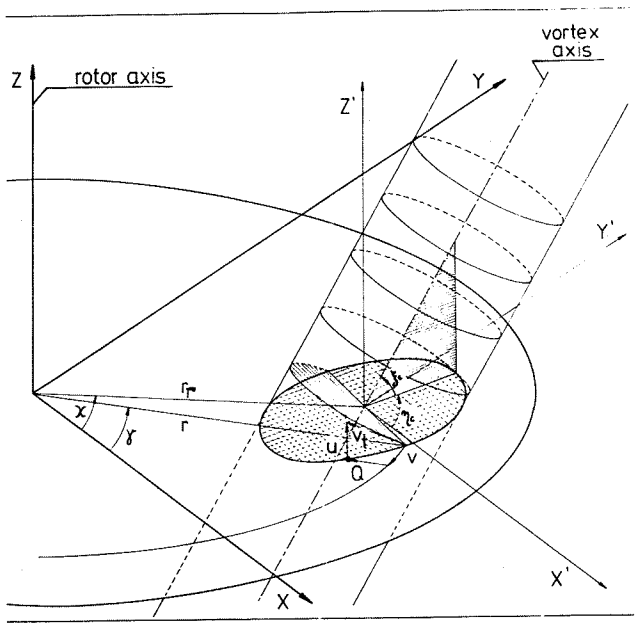

Fig. 24 Velocity perturbation at a point Q caused by a tip vortex whose axis is oblique to the rotor area

The tangential velocity v_t of a vortex is given by Squire (13); v_t depends on the radius r_v and the "age" t_v of the vortex:

$$v_t = \frac{\Gamma}{2\pi r_v}\left(1 - e^{-r_v^2/4\nu_t t_v}\right)$$

Out of a number of experiments Owen (14) found the empirical formula for the eddy viscosity ν_t

$$\frac{\nu_t}{\nu} = 0.588\sqrt{\frac{\Gamma}{\nu}}$$

where $\nu = 15 \cdot 10^{-6}$ m²/s is the kinematic viscosity. The total circulation Γ of the vortex depends on the vortex generator. Using these equations, the shape of the components u and v with respect to the angle γ was computed for a single vortex. The evaluation was carried out with the following parameters: $r_\Gamma = 0.34$ m, $\chi = 180°$, $\Gamma = 10$ m²/s, $t_v = 0.1$ s, $\nu_t = 480\nu$. Fig. 25 shows the shape for four different radial positions r of the rotor.

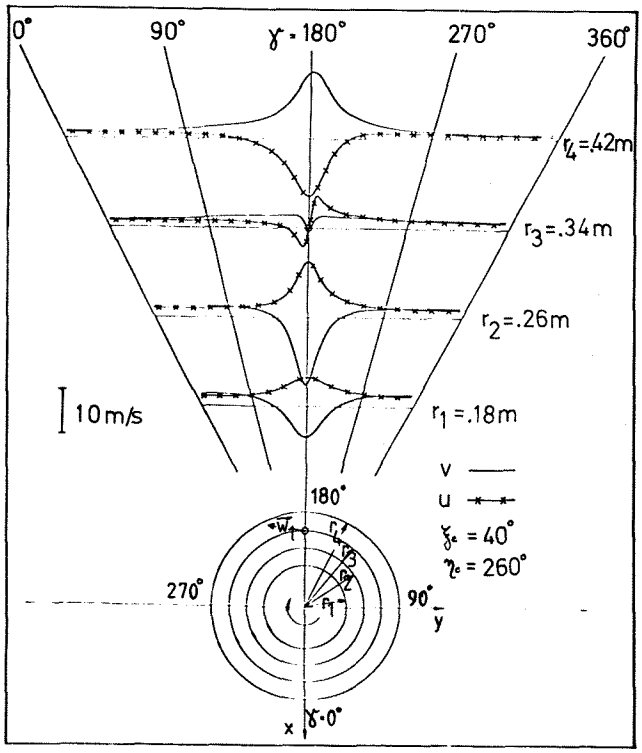

Fig. 25 Shape of the components u and v at four different radial positions

The two vortex spirals outgoing from the two-bladed vortex generator are replaced by a series of line-vortices. The intersections of these vortices with the rotor area are located at the points where the rotor cuts the vortex spirals. The orientation of the axis of the single line vortices is tangential to the vortex spirals. In Fig. 26 the arrangement of the vortex generator relative to the rotor is shown. The positions of the intersections (1a, 2a ... 8a and 1b, 2b ... 8b) have been determined experimentally. Here only a snap shot of the vortex position is shown - the vortex spirals are moving to the left.

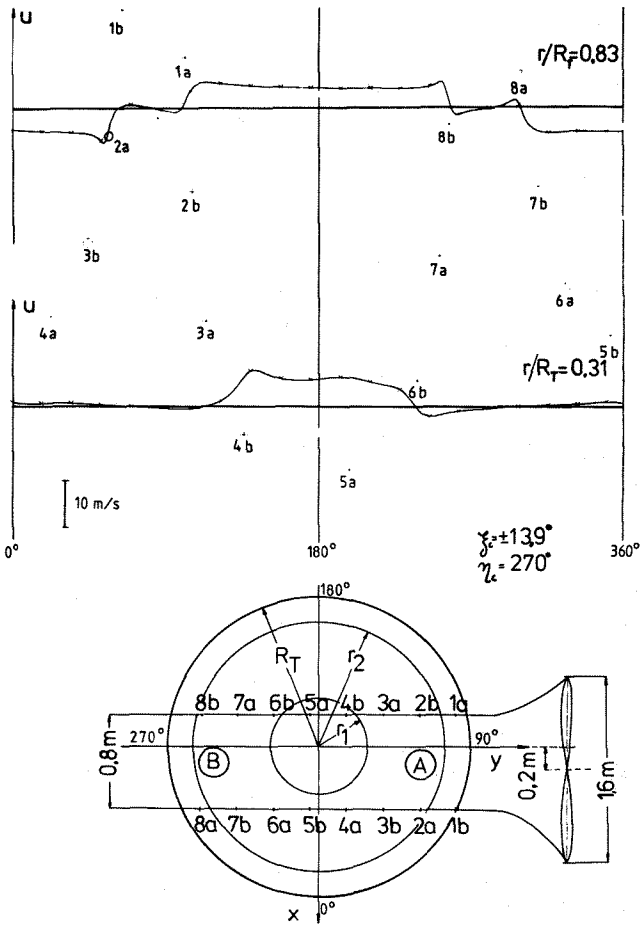

Fig. 26 Shape of the component u with respect to γ generated by the two vortex spirals of the vortex generator

The eddy viscosity ν_t is assumed to be increased during each interaction of a tail rotor blade with the vortex spiral. This increase of ν_t is based on emperical data.

Fig. 27 shows the shape of the tangential velocity v_t for four intersections.

With these assumptions the components u and v were computed as a function of γ at 15 radial positions of the tail rotor. In Fig. 26 the more important component u is shown for r/R_T = 0.83 and r/R_T =.31. Up to now, the unsteady blade forces were computed with the two-dimensional theory of Naumann and Yeh. It is planed to determine the forces by developing a three-dimensional theory following the method given by Fathy (5).

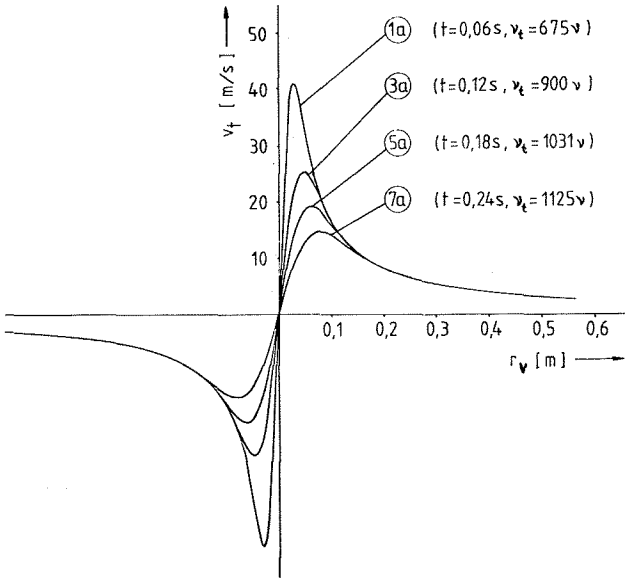

Fig. 27 Peripheral velocity in a vortex spiral of the vortex generator at four different positions (see Fig. 26)

Fig. 28 gives the fourier coefficients K_l of the unsteady blade forces - the parameters correspond to Fig. 26 and the tail rotor speed was n = 1000 rpm.

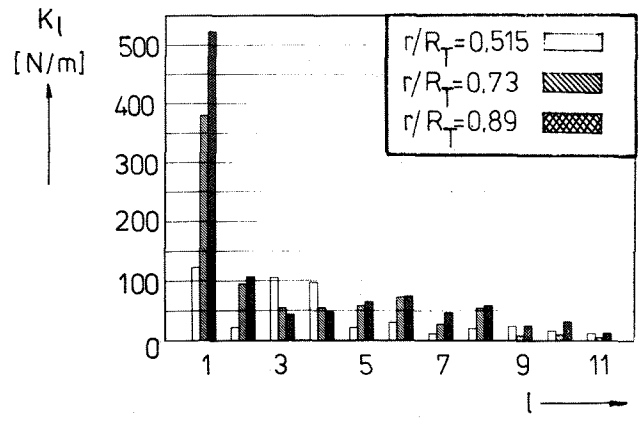

Fig. 28 Fourier coefficients of the blade forces for three radial positions

It can be seen that the force fluctuations increase with the radius r. The same statement was made for a rotor whose inflow was distorted by a wake (compare Fig. 14). Further it can be taken from Fig. 28 that the coefficient K_1 dominates. The reason is that the Fourier coefficient of the component u dominates as well for the harmonic order l = 1 - this can be conducted from Fig. 26.

The local pressure fluctuations were measured with Kulite pressure transducers installed at the radial position r/R_T = 0.83 at 15 % of the chord length. The shape of the instantaneous pressure p in Fig.29 shows two sharp peaks (due to region (A) in Fig. 26) and two broad peaks (due to the vortices with high eddy viscosity ν_t in region (B).

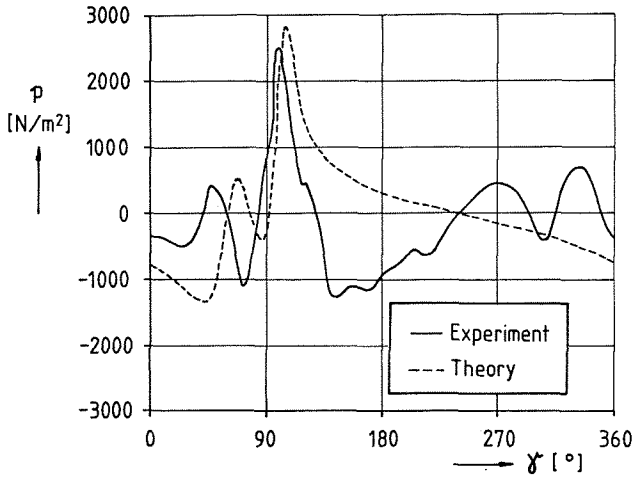

Fig. 29 Pressure fluctuations at a rotor blade during one cycle (r/R_T = 0.83)

The shape of p depends on the position of the moving vortex spirals - the peak at $\gamma \approx 100°$ is generated by a vortex passing very near to the pressure transducer. The pressure shape due to the interactions in region (A) was computed with an extension of the theory of Naumann and Yeh. By adapting the position of the vortex spirals a reasonable agreement with the experimental results could be acchieved.

The influence of the tip vortices on the radiated noise is shown in Fig. 30. The sound pressure levels SPL (overaged across the reverberation room) are plotted versus the frequency f. The undisturbed case (spectrum 1) is shown for comparison with the disturbed inflow (spectrum 2) (vortices corresponding to Fig. 26). The shaft speed of the tail rotor was n = 1000 rpm.

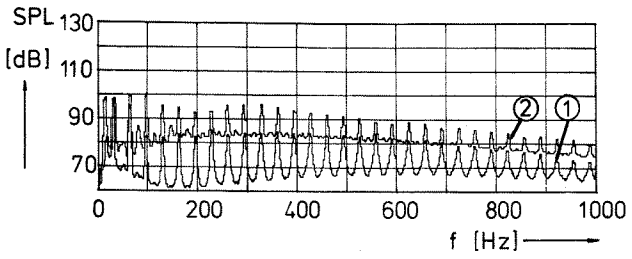

Fig. 30 Sound pressure level spectrum of the tail rotor with distorted inflow (2) and without (1)

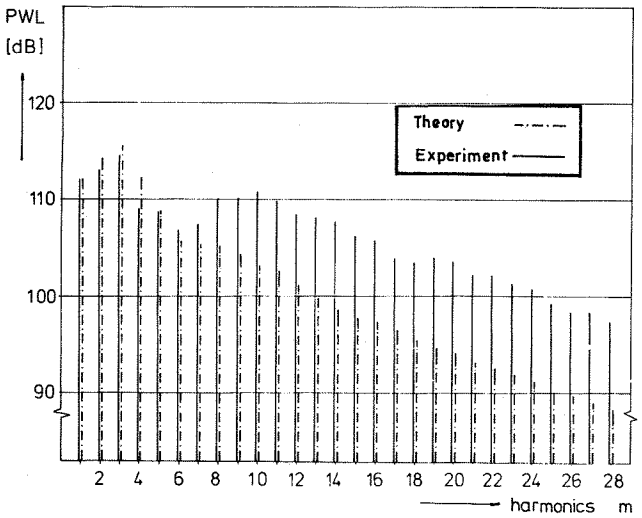

Fig. 31 Computed and measured sound power spectrum of the rotor whose inflow is distorted by tip vortices

In both cases the levels at the blade passage frequency (f = 33.3 Hz) are equal. But due to the vortex spirals the levels of all the harmonics - even of the higher ones - are increased, caused by the fluctuating blade forces containing a high number of harmonics. Besides the levels of the discrete frequency noise the level of the broad-band noise is also increased. That can be explained by the higher turbulence level of the rotor inflow due to the running vortex generator.

Using the sound pressure levels of the discrete frequencies of spectrum 2 in Fig. 30, the corresponding sound power levels were evaluated considering the acoustic characteristics of the reverberation room. In Fig. 31 this power level spectrum is compared with a computed spectrum. According to the theory in chapter 3, the integration over the whole rotor area was carried out - the blade force harmonics were evaluated at 15 radial positions. The computed sound power levels show a good agreement for the blade passage frequency (m = 1) and the harmonics up to m = 7. For the higher harmonics the computed values are too low by the reason explained in the discussion of Fig. 19.

This spectrum was computed with the fixed positions of the vortices 1a, 2a ... 8a and 1b, 2b ... 8b according to Fig. 26. A shift of the vortex spirals over the rotor area has only a negligible influence on the computed noise levels.

5. Conclusions

This paper investigates the influence of two types of inflow distortions on the rotor blade forces and on their increased radiated noise:
case 1: a ducted rotor the inflow of which is distorted by wakes and
case 2: a helicopter tail rotor cutting the tip vortices of the main rotor.

In both cases the measured and computed pressure fluctuations on the rotor blades are periodic and the Fourier analysis shows a high number of harmonics. The computed unsteady blade forces have the same characteristic. For case 1 the unsteady forces have been evaluated with two- and three-dimensional theories. The results of the 3-D-theory show Fourier coefficients of the blade forces with smaller amplitudes compared to those computed with the 2-D-theories. If the wake dont changes in the radial direction of the rotor - as in this paper - the amplitudes of the blade forces become larger with increasing radial position.

The noise theory considers that the Fourier coefficients of the blade forces and their phase relations are changing with the rotor radius. Although this theory only regards the dipole source terms, the measured and computed sound power spectra show a fairly good agreement in the regarded range of the blade tip Mach-Numbers from 0.4 to 0.7. In the noise spectrum especially the harmonics of the blade passage frequency are amplified by the inflow distortions. This causes a strong increase of the subjective loudness.

In case 1 the A-weighted total sound power level is increased up to 18 dBA. The velocity profiles of the wakes can be characterized by the amplitude A, the loss of momentum J_0 and the maximum velocity gradient G. If J_0 is smaller, the loss of momentum is the main factor in determining the fluctuating blade forces and the noise radiation. If J_0 is in-

creased the influence of A dominates. The effect of G is only small.

In case 2 the noise spectrum has a very high number of harmonics of the blade passage frequency. The measured and computed sound power levels at the discrete frequencies are increased by the blade-vortex interaction up to a harmonic order of 50 and more. This is caused by the very impulsive character of the force fluctuations on a blade cutting a vortex. The vortex induces different flow distortions at the blades, where the component normal to the rotor area is the main factor in determining the fluctuating blade forces and the noise radiation.

6. References

1 Kemp, N. H., Sears, W. R., "The Unsteady Forces Due to Viscous Wakes in Turbomachines", Journ. Aeron. Sci., Vol. 22, pp. 478-483, 1955

2 Horlock, J. H., "Fluctuating Lift Forces on Airfoils Moving throug Transverse Chordwise Gusts", Journ. Basic Engineering, Vol. 90, Ser. D Nr. 4, pp 494 - 500, 1968

3 Naumann, H., Yeh, H., "Lift on Pressure Fluctuations of a Cambered Airfoil under Periodic Gusts and Applications in Turbomachinery", Paper 72-GT-30, ASME, 1972

4 Henderson, R. E., "The Unsteady Response of an Axial Flow Turbomachine to an Upstream Disturbance", Ph. D. Thesis, NTIS, AD-759029, 1972

5 Fathy, A. F. A., "The Unsteady Circulation Distribution in Rotors and its Application to Noise Studies", Ph. D. Thesis, South Dakota State Univ., 1973

6 Kellner, A., "Experimentelle und theoretische Untersuchungen über den Einfluß inhomogener Geschwindigkeitsverteilung in der Zuströmung auf die Lärmerzeugung von Mantelschrauben", Ph. D. Thesis, RWTH Aachen, 1980

7 Lighthill, M. J., "On Sound Generated Aerodynamically", Proc. Roy. Soc. A 211, pp 564 - 587, 1952

8 Lowson, M. V., "Theoretical Studies of Compressor Noise". NASA CR-1287, 1969

9 Ollerhead, J. B., Munch, C. L., "An Application of Theory to Axial Compressor Noise". NASA CR-1519, 1970

10 Wright, S. E., "Discrete Radiation from Rotating Periodic Sources". Journ. Sound Vibr., Vol. 17, pp. 437-498, 1971

11 Schreier, J., "Lärmerzeugung von Hubschraubern unter besonderer Berücksichtigung des Heckrotors" Abschlußbericht zum Forschungsauftrag des Landes NRW, Az. IV B3 - FA 8458.

12 VFW - Fokker, "Propellerrechenverfahren-Programm POPAG", 1975

13 Squire, H. B., "The Growth of a Vortex in Turbulent Flow", Aeronautical Quarterly Vol. XVI, p. 302, 1965

14 Owen, P. R., "The Decay of a Turbulent Trailing Vortex", Aeronautical Quarterly Vol. XXI, p. 69, 1970.